ADVANCED MATERIALS
www.advmat.de

Tension-Induced Cavitation in Li-Metal Stripping

Chunyang Wang, Ruoqian Lin, Yubin He, Peichao Zou, Kim Kisslinger, Qi He, Ju Li, and Huolin L. Xin**

Designing stable Li metal and supporting solid structures (SSS) is of fundamental importance in rechargeable Li-metal batteries. Yet, the stripping kinetics of Li metal and its mechanical effect on the supporting solids (including solid electrolyte interface) remain mysterious to date. Here, through nanoscale in situ observations of a solid-state Li-metal battery in an electron microscope, two distinct cavitation-mediated Li stripping modes controlled by the ratio of the SSS thickness (t) to the Li deposit's radius (r) are discovered. A quantitative criterion is established to understand the damage tolerance of SSS on the Li-metal stripping pathways. For mechanically unstable SSS ($t/r < 0.21$), the stripping proceeds via tension-induced multisite cavitation accompanied by severe SSS buckling and necking, ultimately leading to Li "trapping" or "dead Li" formation; for mechanically stable SSS ($t/r > 0.21$), the Li metal undergoes nearly planar stripping from the root via single cavitation, showing negligible buckling. This work proves the existence of an electronically conductive precursor film coated on the interior of solid electrolytes that however can be mechanically damaged, and it is of potential importance to the design of delicate Li-metal supporting structures to high-performance solid-state Li-metal batteries.

1. Introduction

Owing to its high theoretical capacity (3860 mAh g^{-1}) and low electrochemical potential, Li metal in body-centered cubic (BCC) phase (Li_{Metal}) is regarded as the ultimate anode material for high-energy-density rechargeable Li batteries.[1] However, the practical deployments of lithium-metal batteries have long been hampered due to Li_{Metal} morphological instabilities (LMI)[2] in repeated cycling, leading to internal short-circuiting, low Coulombic efficiency, electrolyte consumption, rapid capacity fading, and safety hazards.[3–9] There are two essential problems in Li-metal rechargeable batteries, Li dendrite penetration induced short-circuiting that poses a major safety concern,[10,11] and low Coulombic efficiency that limits cycle life.[12] We propose that the former is caused by compressed Li metal during electrodeposition, while the latter is caused by tensile stress during stripping, which induces cavitation, loss of electronic percolation and dead Li_{Metal}, and fracture and loss of ionic percolation on the solid-electrolyte (SE) side. Despite great advances in elucidating the Li-metal growth mechanisms in the deposition half-cycle,[13,14] so far, the Li-metal kinetics in the stripping half-cycle remain mysterious. Among all the factors that control the Li_{Metal} deposition/stripping, SE interphase (SEI), a solid interface formed between Li_{Metal} and liquid or solid electrolyte is considered to have a critical influence on the morphology and growing/stripping kinetics of Li_{Metal}.[15] Due to electrochemical reductive instability of organic liquid electrolytes at below ≈1 V versus Li^+/Li,[2] the formation of SEI, which is in effect an ad hoc SE nanofilm, is regarded as a necessary evil in order for the liquid-electrolyte battery to function.[16–22] Alternatively, one can use a porous mixed ionic–electronic conductor (MIEC)[11,23,24] which may be absolutely thermodynamically stable against Li_{Metal}, to guide its deposition and stripping and control LMI. Regardless of whether the rechargeable battery uses liquid or solid electrolyte/MIEC,[11,23,24] the issue of tension-driven LMI during stripping is quite universal and requires careful treatment. According to the Nernst equation, if the $U = 0$ V, potential reference (Li^+/Li) is defined based on ambient pressure ($P =$ 1 atm) BCC Li_{Metal}, then a further pressurized Li_{Metal} would shift the equilibrium potential by $U^{eq} = -\Delta P V_{Li}/e$ where $V_{Li} =$ 21.6 Å^3 is the volume of a Li atom in BCC phase and e is the elementary charge,[25,26] since a deposited Li atom would need to work against that additional pressure to be able to join the

C. Wang, Y. He, P. Zou, H. L. Xin
Department of Physics and Astronomy
University of California
Irvine, CA 92697, USA
E-mail: huolin.xin@uci.edu

R. Lin
Chemistry Division
Brookhaven National Laboratory
Upton, NY 11973, USA

K. Kisslinger
Center for Functional Nanomaterials
Brookhaven National Laboratory
Upton, NY 11973, USA

Q. He, J. Li
Department of Nuclear Science and Engineering
Massachusetts Institute of Technology
Cambridge, MA 02139, USA
E-mail: liju@mit.edu

J. Li
Department of Materials Science and Engineering
Massachusetts Institute of Technology
Cambridge, MA 02139, USA

The ORCID identification number(s) for the author(s) of this article can be found under https://doi.org/10.1002/adma.202209091.

DOI: 10.1002/adma.202209091

BCC phase. This means an additional positive pressure of ΔP = 1 MPa locally inside Li_{Metal} in electrodeposition would shift U^{eq} down by 0.135 mV, reducing the overpotential driving force $U^{eq} - U > 0$ and slowing down the deposition. Vice versa, in stripping, if the current is zero (open-circuit condition), with $U^{eq} - U < 0$, a locally negative pressure, or tension, could be autogenerated, and an overpotential of ≈1 mV can, in fact, equilibrate with 7.4 MPa of hydrostatic "tension" locally in the BCC Li_{Metal}. Because the yield strength of Li_{Metal} ranges from MPa to tens of MPa depending on the characteristic sizescale,[27] it is therefore conceivable that even a "small" overpotential on the order of ≈1 mV can generate enough tension to cause cavitation and pull apart the Li_{Metal} from its adhesion with the SSS, or transmit enough stress to damage the SSS itself, including solid-electrolyte components. Damaging the delicate SSS (e.g., SEI) or the contact with SSS (e.g., porosity) will disrupt ionic/electronic transport, and introduce irreversibility in liquid electrolytes or solid SE/MIEC-based Li-metal batteries. This agrees with many empirical observations in the cycling of Li-metal batteries that applying an external pressure on the battery cell on the order of a few MPa[28,29] can greatly improve the cycle life. Such a pressure background P_0 may be added to the local-overpotential-induced tensile ΔP to make the local stress "always" under net compression, to suppress cavitation. However, such an external stack pressure is difficult to engineer at the level of battery pack and takes up extra space and weight. Therefore, it is essential for us to understand tension-induced damage of SSS in Li_{Metal} stripping. This tension may be transmitted to the SEI, which is very thin (thickness t on the order of 10^1–10^2 nm) and fragile, similar to the surface-tension-induced destruction of delicate nanostructures in fluid-phase chemical synthesis. This tension may also be transmitted to the nanoporous solid MIEC structures,[11,23] and damage them as well.

We would like to draw similarities between the creeping Li_{Metal} phase (bulk modulus ≈ 10 GPa) and Newtonian fluids[11,30] such as liquid water (bulk modulus = 2.1 GPa). Cavitation is a widely observed phenomenon in which the static pressure of a liquid reduces to below the liquid's vapor pressure, leading to the formation of a cavity (bubble) completely within the liquid that creates new surfaces, or a cavity at the adhesion interface which debonds wall–liquid interface and creates wall–vapor and liquid–vapor surfaces. While a liquid phase thermodynamically cannot sustain tension, the nucleation of cavities can have a significant kinetic barrier such that liquid water can be seen to sustain hydrostatic tension or negative pressure on the order of 20 MPa for long periods of time.[31] Indeed, for tall trees like *Sequoia sempervirens* to be able to pump groundwater from the root to the crown by capillarity, such tension on the order of MPa must exist inside liquid water and be supported by the surrounding porous solid structures (capillaries inside the tree). When prolific liquid cavitation happens, it can be damaging to the supporting solid structures (SSS) and the entire plant organism.[32] Liquid water cavitation is also damaging to water pumps and propellers, and there is a special category of "cavitation damage" on supporting solid surfaces, due to localized large stresses onto SSS during tension-induced cavitation. Thus, we hypothesize that Li_{Metal} stripping can damage the porous SSS around it, leading to the formation of "dead Li."[33,34] Below, we will show in detail how percolating ionic/electronic transport is disrupted by mechanical damage.

2. Results and Discussion

Resolving these fundamental issues is challenging since it demands both high spatial resolution and the capability of real-time observation. In this work, by constructing a solid-state battery in a transmission electron microscope (TEM) (**Figure 1**a), we directly observed two distinct cavitation-mediated Li stripping pathways controlled by the mechanical stability of the nanoporous SSS, specifically Li_2O. For Li deposits with a high t/r ratio (t is the SEI thickness and r is the whisker radius) of >0.21, the Li deposits strip planarly from the root with negligible SSS buckling (Mode II); in contrast, for Li deposits with a low t/r ratio (< 0.21), the stripping follows a distinctively different pathway whereby severe SSS buckling and necking occur, ultimately leading to Li "trapping" and "dead Li" formation (Mode I) (Figure 1b). It is worth noting that, for both stripping modes, the Li_{Metal} is stripped off through tension-induced cavitation, a phenomenon widely existing in natural plants or man-made pumps (Figure 1c). For mechanically stable Li_2O SSS, the Li stripping nucleation and propagation are enabled by single large cavitation; in contrast, for mechanically unstable Li_2O SSS, the stripping proceeds through multisite cavitation from the Li/Li_2O interface, due to compressive hoop stress $\sigma <$ 0 that exceeds the yield strength of the SSS, $|\sigma| > |\sigma^{Y}_{SSS}|$, which damages the nanoporous SSS. Similar to the cavitation of fluid under tensile stress, e.g., the cavitation of water in a syringe,[35] the cavitations observed here must be driven by the tensile stress autogenerated inside Li_{Metal}, and it also shows similar characteristics as that of the water cavitation.

Figure 2a shows the in situ Li whisker growth inside TEM. Driven by an applied voltage, a Li whisker rapidly grew out of the anode (see the "Experimental Section"). The whisker was intentionally kept in the TEM for minutes for controlled surface oxidation until a layer of SSS, i.e., Li_2O, formed. Figure 2b shows in situ electron diffraction patterns (EDPs) of a Li_{Metal} whisker before and after SSS formation. A diffraction ring corresponding to Li_2O (111) planes is identified. Figure 2c shows a bright-field TEM (BF-TEM) image and EDP of a whisker with a thicker SEI with prolonged oxidation. The strengthened diffraction rings in the EDP indicate the polycrystalline nature of the SEI, which is further validated by high-resolution TEM (HRTEM) (Figure 2d). Electron energy loss spectroscopy (EELS) analyses (Figure 2e,f) confirm the formation of Li_2O on the whisker's surface, while the whisker's interior remains as metallic Li^0.[36] Since Li_2O is the primary inorganic species within the SEI on Li anodes,[37] the Li whisker encapsulated in Li_2O provides a model system to study the Li stripping behavior and its interplay with the delicate SSS.

Figure 3a–h and Movie S1 (Supporting Information) present time-resolved BF-TEM images (contrast inversed) of a Li whisker during stripping. The whisker has a t/r ratio of 0.04, where t is the Li_2O thickness (≈4 nm) and r is the whisker radius (≈100 nm). Upon stripping, two cavities (indicated by the arrows in the insets) nucleated at the Li/Li_2O interface. The stripping rapidly extended toward the interior (stripping fronts

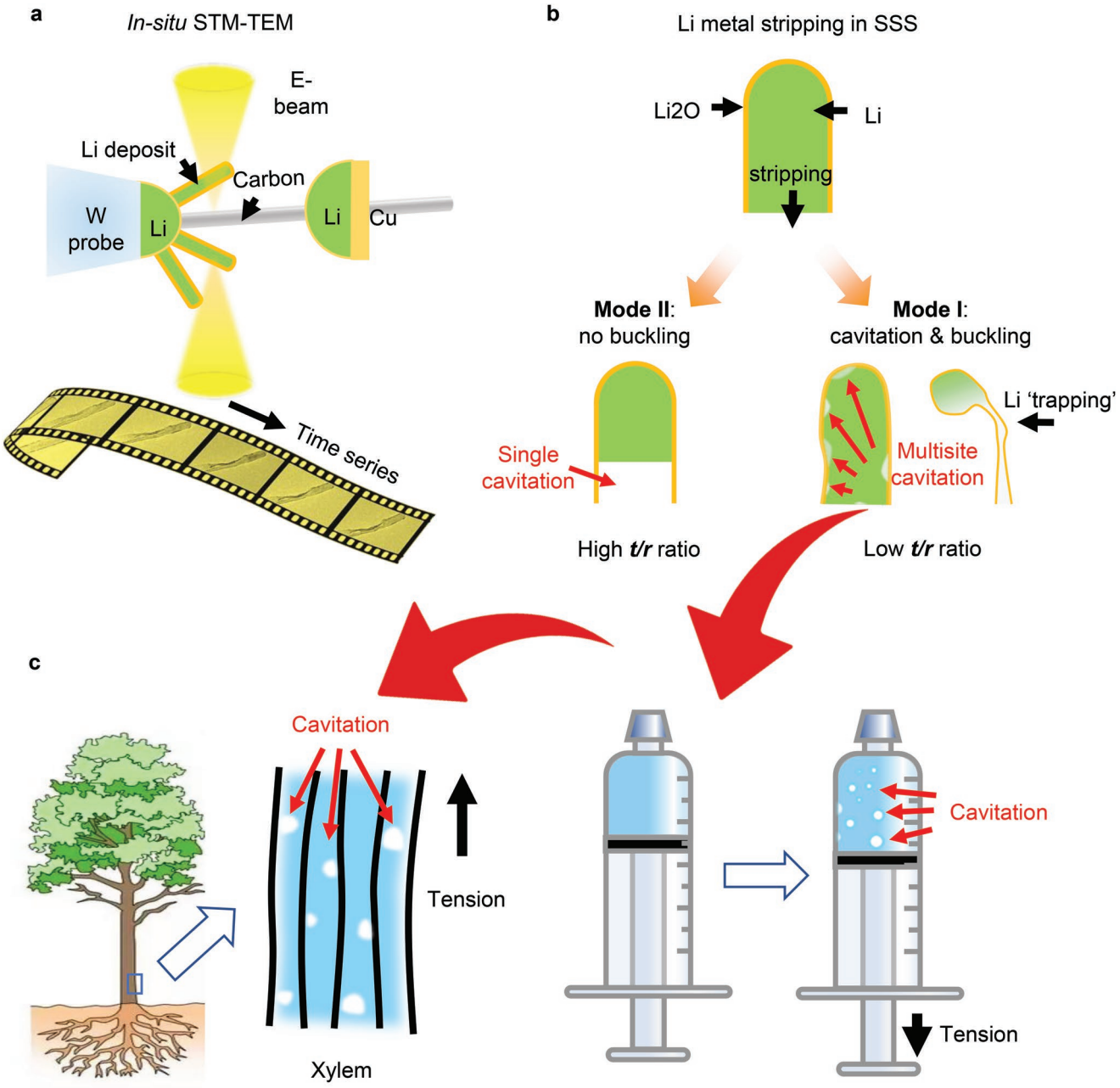

Figure 1. Schematic illustration of the in situ TEM experiment and observed Li stripping pathways. a) Li-metal growth and stripping realized by applying a bias (reversible) between the two electrodes of an STM–TEM probe system, during which time-resolved TEM images are obtained by a CCD camera. A Li_2O film formed on the Li whisker during growth acts as an artificial SE for the following Li stripping. b) Schematics showing the discovered Li whisker stripping modes controlled by the mechanical stability of the Li_2O SE. c) A schematic showing the tension-induced cavitation phenomena in a tree and syringe, analogous to the cavitation of Li metal observed in this work.

are indicated by dash lines) and then another cavity developed at the whisker tip. Subsequently, the Li_2O SSS buckled from the Li-deficient sites during fast Li_{Metal} shrinkage (Figure 3e). This indicates a) significant adhesion force between the SSS and Li_{Metal}, and b) tensile stress originating inside Li_{Metal} is sufficient to pull on and deform an SSS layer of thickness t. Feature (a) was recently corroborated by a cryo-TEM observation, where a zero equilibrium wetting angle was seen between Li_{Metal} and SEI,[38] indicating strong adhesion. The zero wetting angle also means that an undisrupted SEI provides percolating electronic conduction pathway even in stripped condition due to a precursor film[39] of Li^0 adatoms coated on the interior surface, crucial for electrochemical processes. Feature (b) can be derived through the Young–Laplace equation, where the pressure difference between Li_{Metal} and vacuum can be related to the surface tension and radius of curvature R of the cavity, and thus we can show $P(Li_{Metal}) < 0$. As a result, considerable Li_{Metal} was trapped at the whisker tip due to buckling and necking of

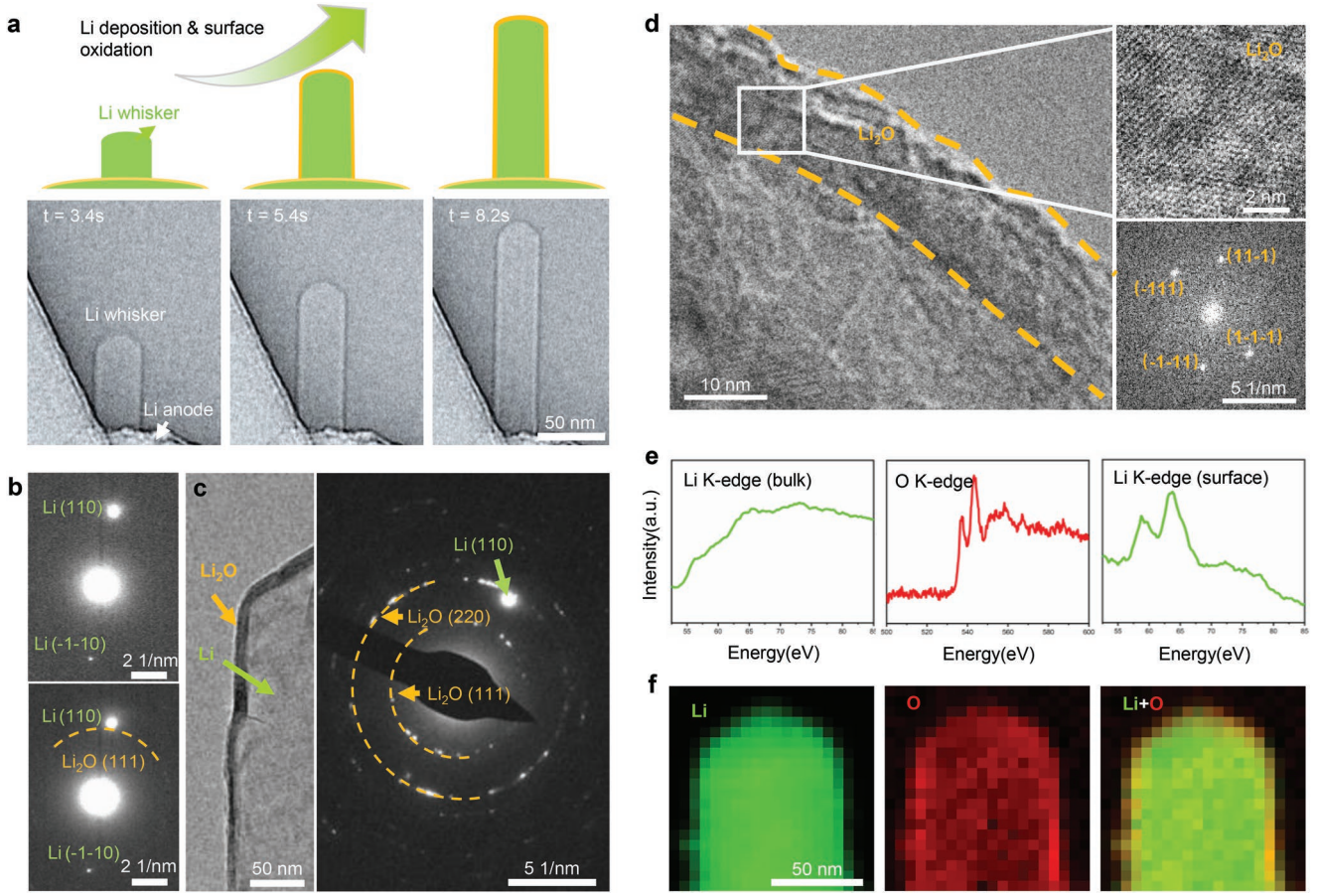

Figure 2. In situ Li_2O solid electrolyte (SE) formation during controlled Li whisker growth and surface oxidation. a) Li whisker growth during in situ Li deposition in TEM. b) In situ electron diffractions of a Li whisker before and after Li_2O SE formation. c) BF-TEM image and EDP of a Li whisker with a thicker Li_2O SE after prolonged oxidation. d) HRTEM image of the Li_2O SE formed on the whisker's surface. e) Electron energy loss spectra of the Li K-edge and O K-edge of a Li whisker. f) EELS maps of Li and O in the Li whisker.

the Li_2O SSS (Figure 3f), which potentially can damage the relatively brittle oxide and affiliated precursor film. After that, the stripping rate of the "trapped" Li_{Metal} was considerably reduced (Figure 3g), although it was completely stripped off with prolonged stripping time (Figure 3h). Figure 3i–l and Movie S2 (Supporting Information) show the stripping dynamics of another Li whisker with a t/r ratio of ≈0.15. It also involves similar SSS buckling, necking, and ultimately Li "trapping", presumably due to the mechanical disruption of the electronically conductive precursor film[39] coated on the interior of the Li_2O shell.[38] In this case, the "trapped" Li was not completely stripped off even after a long period (Figure S1 and see another example in Figure S2 in the Supporting Information), possibly due to the severe necking damage that shuts off electronic and/or ionic transport. Hereafter, this type of Li metal stripping involves severe Li_2O buckling and Li "trapping" is defined as stripping Mode I.

Distinct from the stripping Mode I whereby Li is "trapped" by severely buckled and damaged SSS, another stripping mode was identified in Li whiskers with a higher t/r ratio, thus relatively more robust SSS. **Figure 4**a and Movie S3 (Supporting Information) present the in situ stripping dynamics of a Li whisker with a t/r ratio of ≈0.23. Distinct from Mode I stripping, the stripping of the whisker in Figure 4a started from the root by forming a large cavity rather than multisite cavitation. Subsequently, the cavity extended toward the whisker tip (see EELS maps of a partially stripped whisker in Figure S3 in the Supporting Information), where the Li^0 evacuation must occur by mixed ionic and electronic transport *along* the Li_2O shell with electronically conductive precursor film[39] coated on the inside. Interestingly, the cavity front propagated planarly without SSS buckling throughout the whole process, indicating a new stripping mode (hereafter, denoted as Mode II). No severe inelastic deformation or damage was observed in the Li_2O SSS. Quantitative estimation (Figure 4b) shows that Mode II stripping is nearly linear with time, suggesting that the long-range electronic/ionic transport across a total cavity plug does not seem to present a kinetic limitation. The observation that stripping can continue across a total cavity plug, devoid of any visible Li_{BCC}, is startling; it indicates electronic percolation on the inner surface of the SSS, that is, the inner surface of the Li_2O SSS is MIEC that can adsorb or host Li^0 adatoms, which allows mixed ionic–electronic surface conduction or effectively Li^0 atomic diffusion on the 2D inner surface, even when the bulk Li_{BCC} phase no longer exists to provide electronic percolation. So, the SSS must be a gradient structure with the outer

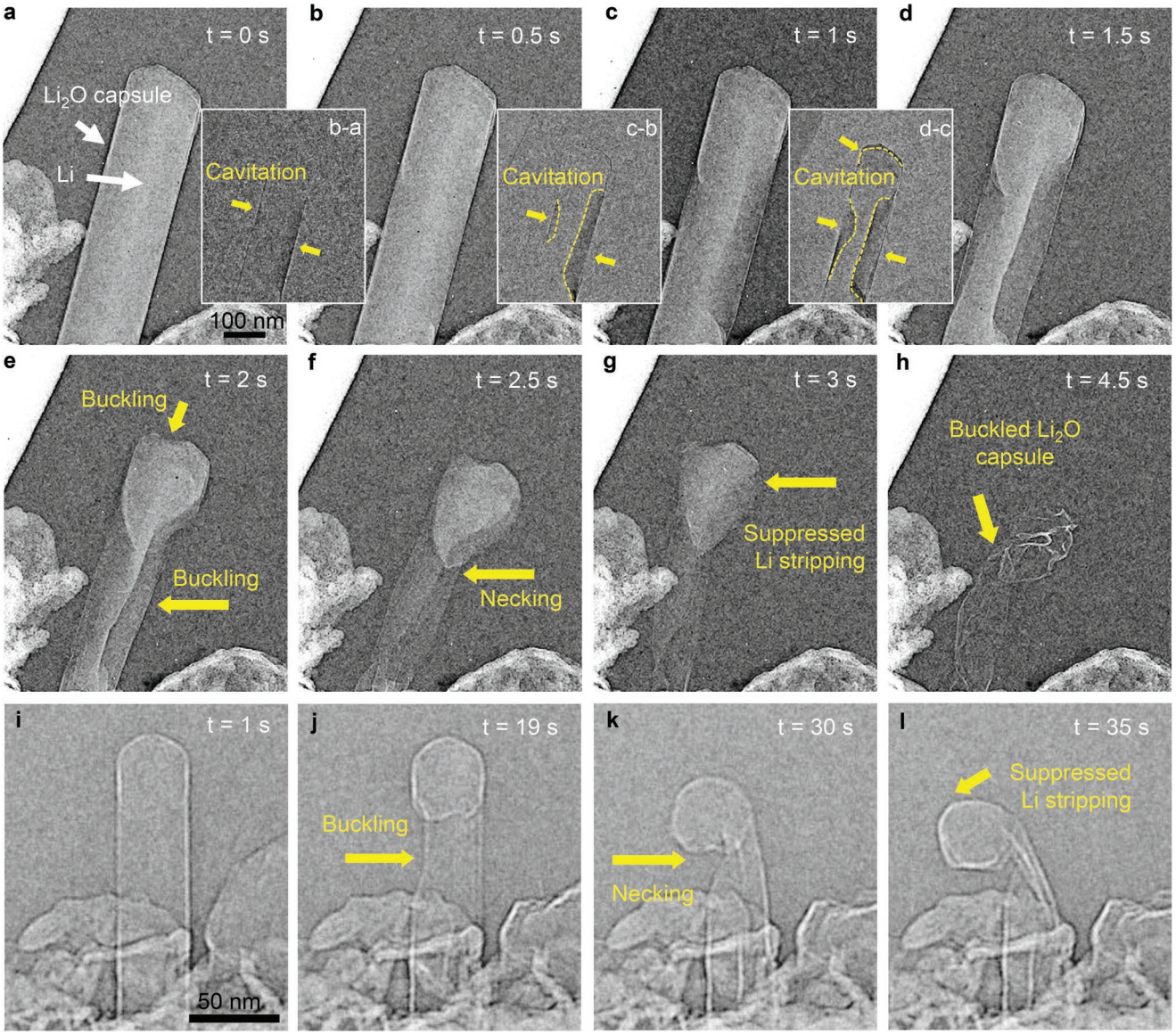

Figure 3. Li stripping via multisite cavitation with nanoporous Li_2O SSS buckling (Mode I). a–h) Time-resolved BF-TEM (contrast inversed) images showing the stripping dynamics of a Li whisker within a Li_2O SSS. Insets show images of panels (b)–(d) subtracted by panel (a)–(c), respectively. The heterogeneous multisite cavitation (yellow arrows) nucleates from the Li/Li_2O interface and extends toward the interior under tension. Further Li stripping leads to buckling and necking of Li_2O, which consequently slows down the Li stripping from the tip. i–l) Stripping dynamics in another Li whisker which shows similar buckling, necking, and Li "trapping."

part being electronically insulating, but the inner surface with a continuous precursor film[39] being highly lithophilic MIEC,[38] as long as it is not mechanically cracked/damaged. Mode II or total cavity plug stripping has also been seen in other open porous MIEC SSS.[11] Our observations prove the electronic insulator-to-electronic conductor gradient structure of the Li_2O-based SEI layer and provide an inner logical link between liquid-electrolyte SEI[38] and 2D/3D MIEC SSS for both liquid- and solid-state Li-metal batteries.

Figure 4c shows a similar stripping pathway (Mode II) as shown in Figure 4a. In addition, stripping Mode II was also observed in ultralong whiskers (Figure S4, Supporting Information), which indicates that long-distance MIEC diffusion on the inner surface of SEI is possible, as long as the SEI is not mechanically damaged. Figure 4d shows a whisker with a nonuniform diameter. Since the bottom part has a considerably smaller t/r ratio, it underwent severe buckling (stripping Mode I) while the tip obeys Mode II stripping. Figure 4e shows the statistical distribution of the two stripping modes according to the SSS thickness (t) and whisker radius (r). The data points can be divided into two distinct domains by a critical line with a t/r ratio of 0.21. This is consistent with our observations that for whiskers with a t/r ratio of 0.21, the SSS only shows moderate buckling without necking or Li_{Metal} "trapping" (Figure S5, Supporting Information). From the above, the Li stripping mechanism in Li_2O SSS is summarized as follows: for whiskers with

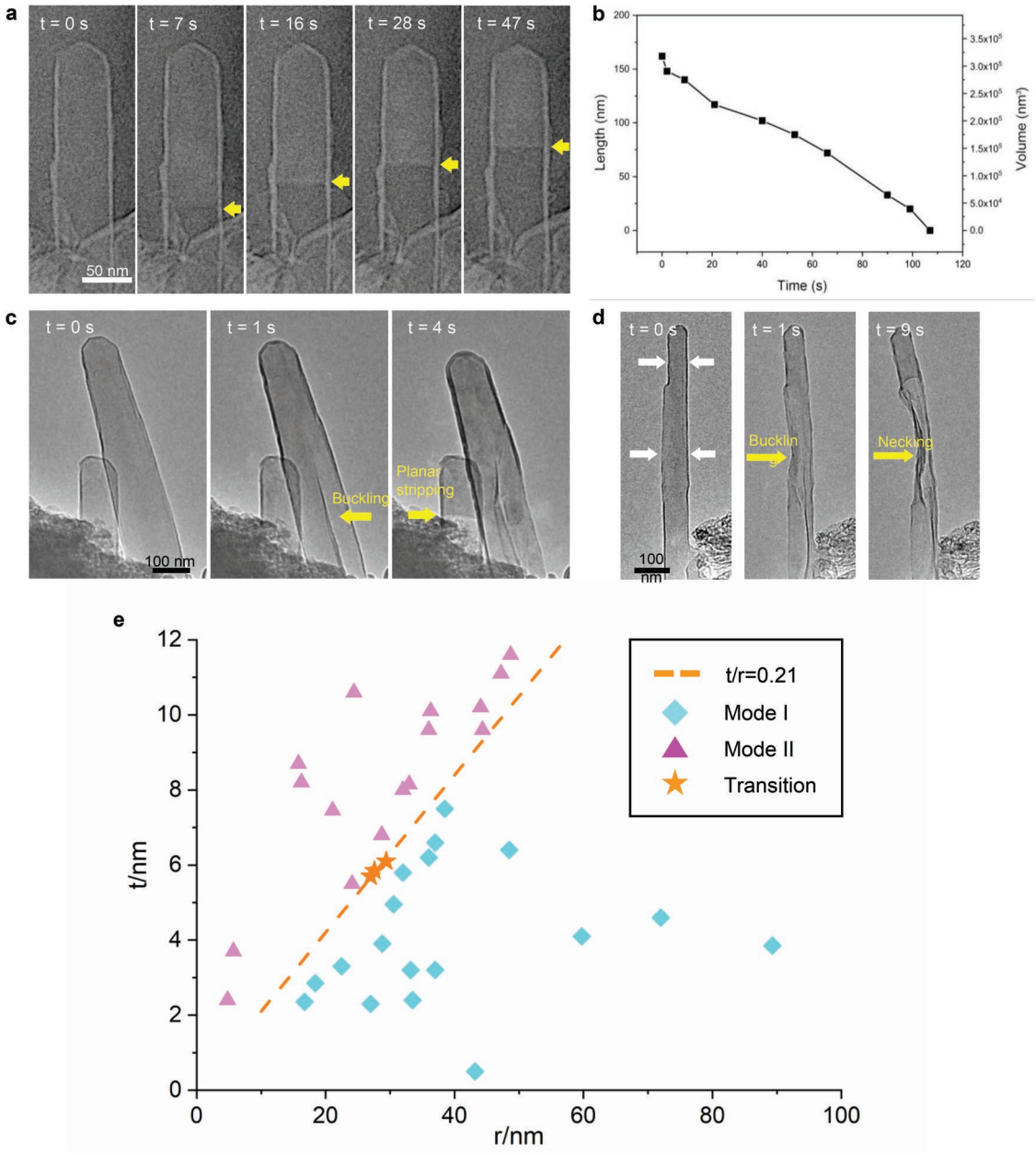

Figure 4. Li stripping via single cavitation in mechanically stable Li_2O SSS (Mode II). a) Time-resolved BF-TEM (contrast-inversed) images showing the stripping dynamics of a Li whisker within a Li_2O SSS. The stripping started from the root and extended planarly toward the tip of the whisker. b) The length and volume of the whisker in panel (a) as a function of time, which shows a nearly linear stripping with time. c) Mode II stripping in a whisker with a larger diameter. d) Mixed stripping modes in a whisker with nonuniform diameters. The bottom of the SE tube underwent severe buckling (Mode I), while the tip remained stable (Mode II). e) Statistical distribution of the two stripping modes. Mode I and Mode II are denoted by cyan diamonds and magenta triangles, respectively, separated by a critical line with a t/r ratio of 0.21. The data points of transition modes are denoted by stars. The sample size (n) for the statistical analysis is 37.

a low t/r ratio (<0.21), the stripping follows Mode I whereby the Li strips inhomogeneously with severe SSS buckling and damage, which leads to Li "trapping," fundamentally causing irreversibility of Li-metal batteries that rely on delicate SEI or SSS in order to function electrochemically; for Li whiskers with a high t/r ratio (>0.21), the Li stripping follows stripping Mode II, whereby the Li strips planarly with no SSS buckling or damage. The mechanical criterion and stripping mechanism are expected to be applicable to lithium-ion batteries either with solid-state electrolytes or conventional liquid electrolytes because almost all forms of Li deposits have the same core–shell structure (Li metal covered by SEI shell). For example, we performed in situ deposition–stripping experiments with a practical solid electrolyte—$Li_{1.3}Al_{0.3}Ti_{1.7}(PO_4)_3$ (LATP). Figure S6a (Supporting Information) shows the TEM setup for the in situ Li deposition/stripping experiment with the LATP system.

During the in situ Li stripping process, both stripping Mode I (Figure S6b, Supporting Information) and Mode II (Figure S6c, Supporting Information) were observed. Figure S7 (Supporting Information) shows statistical distribution of the two types of stripping modes by including the new data points (the hollow symbols are data points obtained from the LATP) in Figure 4. The result demonstrates that the mechanical criterion established in this work is basically applicable to practical solid electrolytes. It is worth noting that SSS are broader concepts for the interfaces with Li_{Metal}, including but also extending beyond, the notion of SEI. SSS/SEI are all mechanically delicate structures that need to survive Li_{Metal} cycling. Mode II Li^0 stripping proves a generic conclusion that the Li_2O SSS sheath interior is metallic and allows 2D or interfacial MIEC conduction. So Li-metal batteries, regardless of liquid electrolyte SEI or SE/SSS, work on the inside as 2D MIEC, and as long as the SSS with metallic precursor film[39] coated on the inside are not mechanically damaged.

According to the elasticity solution of a cylindrical pressure vessel, the in-plane stress inside the tubular SSS of thickness t should be[40]

$$\sigma = (\Delta P) r / t \tag{1}$$

where ΔP is the pressure difference across the pressure vessel wall, and r is the radius of the Li_{Metal}. We hypothesize that once ΔP is large enough, σ exceeds the yield strength σ^{Y}_{SSS} of Li_2O SSS (see a schematic illustration in **Figure 5**). This is quite similar to the cavitation of liquid water under tension.[31] Liquid water can sustain tension before cavitation of about 20 MPa

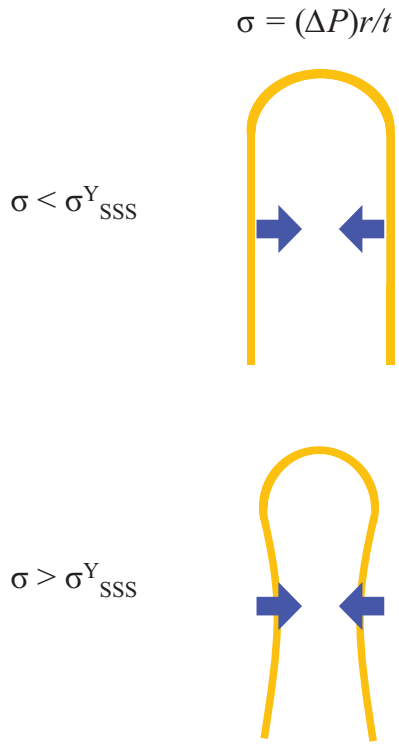

Figure 5. Schematic illustration of the mechanical criterion for the failure of SSS.

(the bulk modulus of liquid water is 2.1 GPa). For Li metal, which has a bulk modulus of ≈10 GPa, it is possible that it can sustain a hydrostatic tension of ≈100 MPa before cavitation (if converted to overpotential, it would be on the order of 13 mV). According to the criterion, the compressive stress inside Li_2O is amplified by r/t in a cylindrical pipe. Therefore, when cavitation is activated during stripping, the compressive stress in the Li_2O pressure-vessel wall is estimated as ≈500 MPa. This suggests that 500 MPa is beyond the compressive yield strength σ^{Y}_{SSS} of Li_2O, consistent with the estimated yield stress of Li_2O (the Young's modulus of Li_2O is 108 GPa,[41] so if there is no yield, 0.5% elastic strain should be sustained, but most materials can only sustain 0.2–0.5% elastic strain at room temperature, especially for materials like the SE with many flaws. The high-temperature creep strength of Li_2O at 700–800 °C is in the range of 15–45 MPa[41]). Therefore, it is reasonable to conclude that when the compression exceeds the σ^{Y}_{SSS} of Li_2O, it plastically crumples due to large negative σ and, consequently, the electronic percolation on its inner surface MIEC is disrupted. Since Li_2O is a dominant component[37] in SEI, the quantitative understanding of the mechanical failure of Li_2O will be valuable for the design of SEI from a mechanical perspective, and for mixed-conducting SSS in general.

Whisker is not the only form of Li morphologies. For example, chunky Li such as Li dome is also common morphology of Li deposits. Despite the difference in their geometries, all of them share the same core–shell structure—Li metal covered by SSS. Therefore, in principle, Li deposits with other morphologies are expected to show similar behaviors in terms of the mechanical stability of the SEI during Li stripping. Therefore, we expect the quantitative criterion (the t/r ratio may vary for different geometries) uncovered in Li whiskers should also be applicable to other forms of Li deposits. A statistical study on the stripping of other forms of Li deposits and corresponding critical t/r ratios could be performed in the near future. Yet, we would like to emphasize that the scenario for practical batteries is much more complicated than the simplified case demonstrated in this work. First, the "real" SEI is not composed of a single component/phase. The SEI components derived from different electrolyte systems are different. Second, the morphologies of Li deposits vary from one electrolyte to another. Third, even for one specific electrolyte system, multiple morphologies (e.g., whiskers, domes, and mosaic structures) are usually involved. In one word, the t/r ratio, in principle, could be transferred to practical batteries as the ratio between the SSS thickness and the Li deposit's size. However, a unified (therefore, more complicated) model with considering all the above-mentioned factors requires more work to be done in the future. In addition, the applied current density/potential could possibly change the exact value of the t/r ratio. We do not expect that the exact t/r ratio of 0.21 in the simplified case in this work will be generally applicable to all occasions, but we believe the stripping mode transition and the mechanical criterion uncovered in our work will qualitatively hold.

Our work provides a general understanding of the cycling behavior of Li metal inside supporting solid structures in Li-metal batteries. In this work, $Li_{Metal}@Li_2O$ is used as a model system to quantitatively understand the influence of the mechanical stability of SSS on the Li-metal stripping pathways.

We show that for a whisker with a t/r ratio smaller than a certain value, the stripping proceeds via multisite cavitation accompanied by severe buckling, necking, and ultimately Li "trapping"; while, for whiskers with a t/r ratio larger than a critical value, the Li_{Metal} undergoes planar stripping and negligible SE buckling. The value of 0.21 is specific to the case of Li_{Metal}@Li_2O; however, the concept established in the work is expected to apply to a variety of battery systems involving porous MIEC SSS or the formation of SEI on the metallic deposits. To ensure stable function of SSS, its yield strength and ductility are key. Our work provides a damage criterion that may find important implications. From the above, it is clear that a smaller r (if t is fixed) is preferred in terms of obtaining good rate capability and cycling damage tolerance, yet, at the sacrifice of net storage capacity due to the formation of electrochemically inactive SSS. This suggests that to design a Li-metal battery to achieve the best capacity-rate/cycle life balance, we need to choose r wisely in order to ensure undisrupted ionic/electronic transport from SSS.

3. Conclusion

In conclusion, by using nanoscale in situ TEM observations, we decipher the cavitation-induced Li-metal stripping inside a supporting solid structure. Two distinct stripping pathways determined by the length-scale controlled mechanical stability of Li_2O SE are uncovered. A mechanical criterion, i.e., t/r ratio is proposed to quantitatively understand the interplay between the SE's mechanical stability and the Li stripping kinetics. Our work provides a fundamental understanding of the stripping behaviors of Li metal inside supporting solid structures, and it opens a new avenue to better control the "dead Li" formation in Li-metal batteries by regulating the length scales of supporting solid structures that provide dimensional stability and ionic/electronic transport.

4. Experimental Section

In Situ TEM Experiments: In situ experiments (see a schematic illustration of the experimental procedure in Figure S8 in the Supporting Information) were performed by using a Nanofactory scanning tunneling microscopy (STM)–TEM setup[42] in an FEI Talos F200X transmission electron microscope with an X-FEG field emission source. First, a copper wire (with a flat tip) attached to dozens of individual carbon fibers was prepared via triboelectric attractive force (the electrostatic charge was introduced to the copper wire by the friction between the copper wire and a tweezer), serving as a fixed electrode for the system. Next, an STM W probe with a scratch of Li metal on the probe tip was prepared by scratching off a small amount of Li metal from a Li ribbon. Later on, the W tip with Li metal was left in the air for around 5 s to introduce a thin (≈100 nm thick) SSS mainly composed of Li_2O on the surface of the Li metal. The W probe was then loaded onto a piezocontrolled copper hat, serving as the other electrode for the system. The functionalized carbon fiber which acts as an MIEC was made to contact the Li_2O@Li driven by precise piezoforce control, first with a coarse step and then with a fine step of 1 nm. (The carbon fiber was purchased from XFNANO. The functionalization of the surface was achieved by heating the carbon fibers in concentrated nitric acid at 80 degrees Celsius for 5 hours. The fibers were cleaned and dryed by repeated centrifuging followed by freeze drying). The Li deposition or stripping processes were achieved under a constant bias of 5/−5 V between the two electrodes. The microscope was operated at 200 kV, with an extraction voltage of 3850 V, the gun lens of 4, the spot size of 6, the C1 aperture size of 2000 µm, and the C2 aperture size of 70 µm. Low-dose imaging with a dose rate of ≈0.5 e $Å^{-2}$ s^{-1} was adopted to avoid beam damage during the in situ experiments. Note that no independent experiments were designed to obtain each data point with a certain r/t ratio; otherwise, multiple whiskers were grown from the anode in one plating process. Due to the fact that the growth kinetics of different whiskers are different (varied nucleation time, growth rate, diameters, etc.), the data points were obtained with different combinations of r and t for the statistical analysis.

Supporting Information

Supporting Information is available from the Wiley Online Library or from the author.

Acknowledgements

C.W., R.L., and Y.H. contributed equally to this work. This work was supported by the Materials Science and Engineering Divisions, Office of Basic Energy Sciences of the U.S. Department of Energy, under Award No. DE-SC0021204. J.L. acknowledges support by NSF CBET-2034902 and DARPA MINT program under contract number HR001122C0097. R.L. was supported by the Assistant Secretary for Energy Efficiency and Renewable Energy, Vehicle Technology Office of the U.S. Department of Energy through the Advanced Battery Materials Research (BMR) Program, including Battery500 Consortium under Contract DE-SC0012704. This research used resources of the Center for Functional Nanomaterials (CFN), which is a U.S. Department of Energy Office of Science User Facility, at Brookhaven National Laboratory under Contract No. DE-SC0012704. The authors thank Sooyeon Hwang for her support of the TEM experiments.

Conflict of Interest

The authors declare no conflict of interest.

Data Availability Statement

The data that support the findings of this study are available from the corresponding author upon reasonable request.

Keywords

in situ TEM, mechanical damage, mixed ionic–electronic conductor, precursor film, solid electrolyte

Received: October 3, 2022
Revised: November 5, 2022
Published online: December 16, 2022

[1] K. Yan, Z. Lu, H.-W. Lee, F. Xiong, P.-C. Hsu, Y. Li, J. Zhao, S. Chu, Y. Cui, *Nat. Energy* **2016**, *1*, 16010.
[2] S. Li, M. Jiang, Y. Xie, H. Xu, J. Jia, J. Li, *Adv. Mater.* **2018**, *30*, 1706375.
[3] H. Liu, X.-B. Cheng, J.-Q. Huang, H. Yuan, Y. Lu, C. Yan, G.-L. Zhu, R. Xu, C.-Z. Zhao, L.-P. Hou, C. He, S. Kaskel, Q. Zhang, *ACS Energy Lett.* **2020**, *5*, 833.

[4] X. Gao, Y.-N. Zhou, D. Han, J. Zhou, D. Zhou, W. Tang, J. B. Goodenough, *Joule* **2020**, *4*, 1864.
[5] J. Kasemchainan, S. Zekoll, D. S. Jolly, Z. Ning, G. O. Hartley, J. Marrow, P. G. Bruce, *Nat. Mater.* **2019**, *18*, 1105.
[6] F. Han, A. S. Westover, J. Yue, X. Fan, F. Wang, M. Chi, D. N. Leonard, N. J. Dudney, H. Wang, C. Wang, *Nat. Energy* **2019**, *4*, 187.
[7] X. Liu, R. Garcia-Mendez, A. R. Lupini, Y. Cheng, Z. D. Hood, F. Han, A. Sharafi, J. C. Idrobo, N. J. Dudney, C. Wang, C. Ma, J. Sakamoto, M. Chi, *Nat. Mater.* **2021**, *20*, 1485.
[8] P. Zou, Y. Wang, S. W. Chiang, X. Wang, F. Kang, C. Yang, *Nat. Commun.* **2018**, *9*, 464.
[9] R. Lin, Y. He, C. Wang, P. Zou, E. Hu, X. Q. Yang, K. Xu, H. L. Xin, *Nat. Nanotechnol.* **2022**, *17*, 768.
[10] P. Zou, Y. Sui, H. Zhan, C. Wang, H. L. Xin, H.-M. Cheng, F. Kang, C. Yang, *Chem. Rev.* **2021**, *121*, 5986.
[11] Y. Chen, Z. Wang, X. Li, X. Yao, C. Wang, Y. Li, W. Xue, D. Yu, S. Y. Kim, F. Yang, A. Kushima, G. Zhang, H. Huang, N. Wu, Y.-W. Mai, J. B. Goodenough, J. Li, *Nature* **2020**, *578*, 251.
[12] Y. He, P. Zou, S.-M. Bak, C. Wang, R. Zhang, L. Yao, Y. Du, E. Hu, R. Lin, H. L. Xin, *ACS Energy Lett.* **2022**, *7*, 2866.
[13] Y. He, X. Ren, Y. Xu, M. H. Engelhard, X. Li, J. Xiao, J. Liu, J. G. Zhang, W. Xu, C. Wang, *Nat. Nanotechnol.* **2019**, *14*, 1042.
[14] L. Zhang, T. Yang, C. Du, Q. Liu, Y. Tang, J. Zhao, B. Wang, T. Chen, Y. Sun, P. Jia, H. Li, L. Geng, J. Chen, H. Ye, Z. Wang, Y. Li, H. Sun, X. Li, Q. Dai, Y. Tang, Q. Peng, T. Shen, S. Zhang, T. Zhu, J. Huang, *Nat. Nanotechnol.* **2020**, *15*, 94.
[15] Y. Li, W. Huang, Y. Li, A. Pei, D. T. Boyle, Y. Cui, *Joule* **2018**, *2*, 2167.
[16] B. Wu, S. Wang, J. Lochala, D. Desrochers, B. Liu, W. Zhang, J. Yang, J. Xiao, *Energy Environ. Sci.* **2018**, *11*, 1803.
[17] Q. Tu, L. Barroso-Luque, T. Shi, G. Ceder, *Cell Rep. Phys. Sci.* **2020**, *1*, 100106.
[18] Y.-K. Sun, P. V. Kamat, *ACS Energy Lett.* **2021**, *6*, 2356.
[19] H. Wu, H. Jia, C. Wang, J.-G. Zhang, W. Xu, *Adv. Energy Mater.* **2021**, *11*, 2003092.
[20] Z. Wang, F. Qi, L. Yin, Y. Shi, C. Sun, B. An, H. M. Cheng, F. Li, *Adv. Energy Mater.* **2020**, *10*, 1903843.
[21] Z. Wang, C. Sun, Y. Shi, F. Qi, Q. Wei, X. Li, Z. Sun, B. An, F. Li, *J. Power Sources* **2019**, *439*, 227073.
[22] B. Han, D. Feng, S. Li, Z. Zhang, Y. Zou, M. Gu, H. Meng, C. Wang, K. Xu, Y. Zhao, H. Zeng, C. Wang, Y. Deng, *Nano Lett.* **2020**, *20*, 4029.
[23] Z. Wang, X. Li, Y. Chen, K. Pei, Y.-W. Mai, S. Zhang, J. Li, *Chem* **2020**, *6*, 2878.
[24] R. J. Y. Park, C. M. Eschler, C. D. Fincher, A. F. Badel, P. Guan, M. Pharr, B. W. Sheldon, W. C. Carter, V. Viswanathan, Y.-M. Chiang, *Nat. Energy* **2021**, *6*, 314.
[25] S. Kim, S. J. Choi, K. Zhao, H. Yang, G. Gobbi, S. Zhang, J. Li, *Nat. Commun.* **2016**, *7*, 10146.
[26] W. Xue, T. Chen, Z. Ren, S. Y. Kim, Y. Chen, P. Zhang, S. Zhang, J. Li, *Appl. Energy* **2020**, *273*, 115230.
[27] C. D. Fincher, D. Ojeda, Y. Zhang, G. M. Pharr, M. Pharr, *Acta Mater.* **2020**, *186*, 215.
[28] R. Weber, M. Genovese, A. J. Louli, S. Hames, C. Martin, I. G. Hill, J. R. Dahn, *Nat. Energy* **2019**, *4*, 683.
[29] Y.-G. Lee, S. Fujiki, C. Jung, N. Suzuki, N. Yashiro, R. Omoda, D.-S. Ko, T. Shiratsuchi, T. Sugimoto, S. Ryu, J. H. Ku, T. Watanabe, Y. Park, Y. Aihara, D. Im, I. T. Han, *Nat. Energy* **2020**, *5*, 299.
[30] C. Herring, *J. Appl. Phys.* **1950**, *21*, 437.
[31] A. S. Henderson, R. Speedy, *J. Phys. E: Sci. Instrum.* **1980**, *13*, 778.
[32] H. Cochard, *C. R. Phys.* **2006**, *7*, 1018.
[33] Y. Liu, D. Lin, P. Y. Yuen, K. Liu, J. Xie, R. H. Dauskardt, Y. Cui, *Adv. Mater.* **2017**, *29*, 1605531.
[34] C. Fang, J. Li, M. Zhang, Y. Zhang, F. Yang, J. Z. Lee, M. H. Lee, J. Alvarado, M. A. Schroeder, Y. Yang, B. Lu, N. Williams, M. Ceja, L. Yang, M. Cai, J. Gu, K. Xu, X. Wang, Y. S. Meng, *Nature* **2019**, *572*, 511.
[35] J.-C. Veilleux, K. Maeda, T. Colonius, J. E. Shepherd, in *Proc. of the 10th Symp. on Cavitation (CAV2018)*, New York **2018**, p. 1068.
[36] F. Wang, J. Graetz, M. S. Moreno, C. Ma, L. Wu, V. Volkov, Y. Zhu, *ACS Nano* **2011**, *5*, 1190.
[37] W. Huang, H. Wang, D. T. Boyle, Y. Li, Y. Cui, *ACS Energy Lett.* **2020**, *5*, 1128.
[38] B. Han, X. Li, Q. Wang, Y. Zou, G. Xu, Y. Cheng, Z. Zhang, Y. Zhao, Y. Deng, J. Li, M. Gu, *Adv. Mater.* **2022**, *34*, 2108252.
[39] J. Y. Huang, Y.-C. Lo, J. J. Niu, A. Kushima, X. Qian, L. Zhong, S. X. Mao, J. Li, *Nat. Nanotechnol.* **2013**, *8*, 277.
[40] L. W. McKeen, in *Fatigue and Tribological Properties of Plastics and Elastomers*, William Andrew, Amsterdam **2016**, p. 1.
[41] M. C. Billone, Y. Y. Liu, R. B. Poeppel, J. L. Routbort, K. C. Goretta, D. S. Kupperman, *J. Nucl. Mater.* **1986**, *141–143*, 282.
[42] C. Wang, K. Du, K. Song, X. Ye, L. Qi, S. He, D. Tang, N. Lu, H. Jin, F. Li, H. Ye, *Phys. Rev. Lett.* **2018**, *120*, 186102.

ADVANCED MATERIALS

Supporting Information

for *Adv. Mater.,* DOI: 10.1002/adma.202209091

Tension-Induced Cavitation in Li-Metal Stripping

Chunyang Wang, Ruoqian Lin, Yubin He, Peichao Zou, Kim Kisslinger, Qi He, Ju Li, and Huolin L. Xin**

Supporting Information

Tension-induced cavitation in Li metal stripping

Chunyang Wang[1], Ruoqian Lin[2], Yubin He[1], Peichao Zou[1], Kim Kisslinger[3], Qi He[4], Ju Li[4,5], Huolin L. Xin[1]**

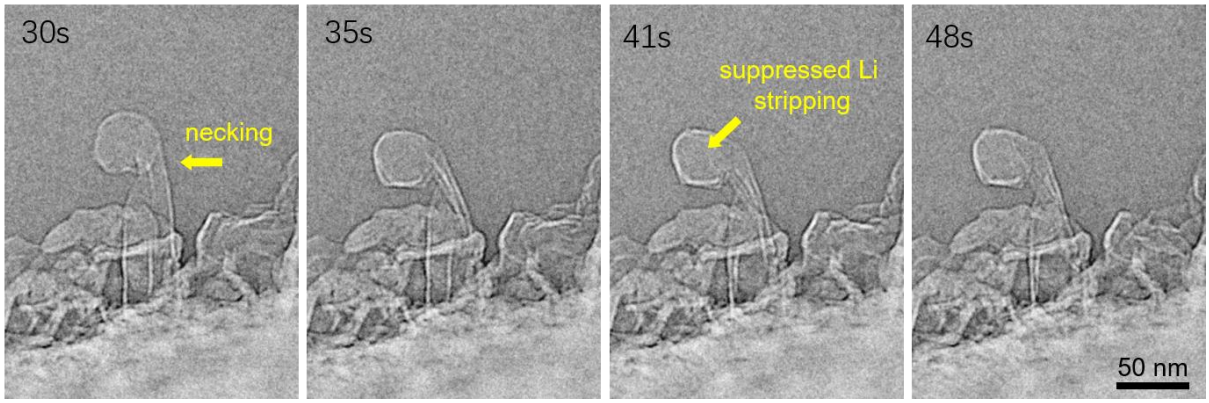

Figure S1. *In-situ* observation of stripping Mode I corresponding to that shown in Figure 1i-l. Severe SEI buckling and necking and Li 'trapping' was observed during the stripping process. The applied bias is -5V.

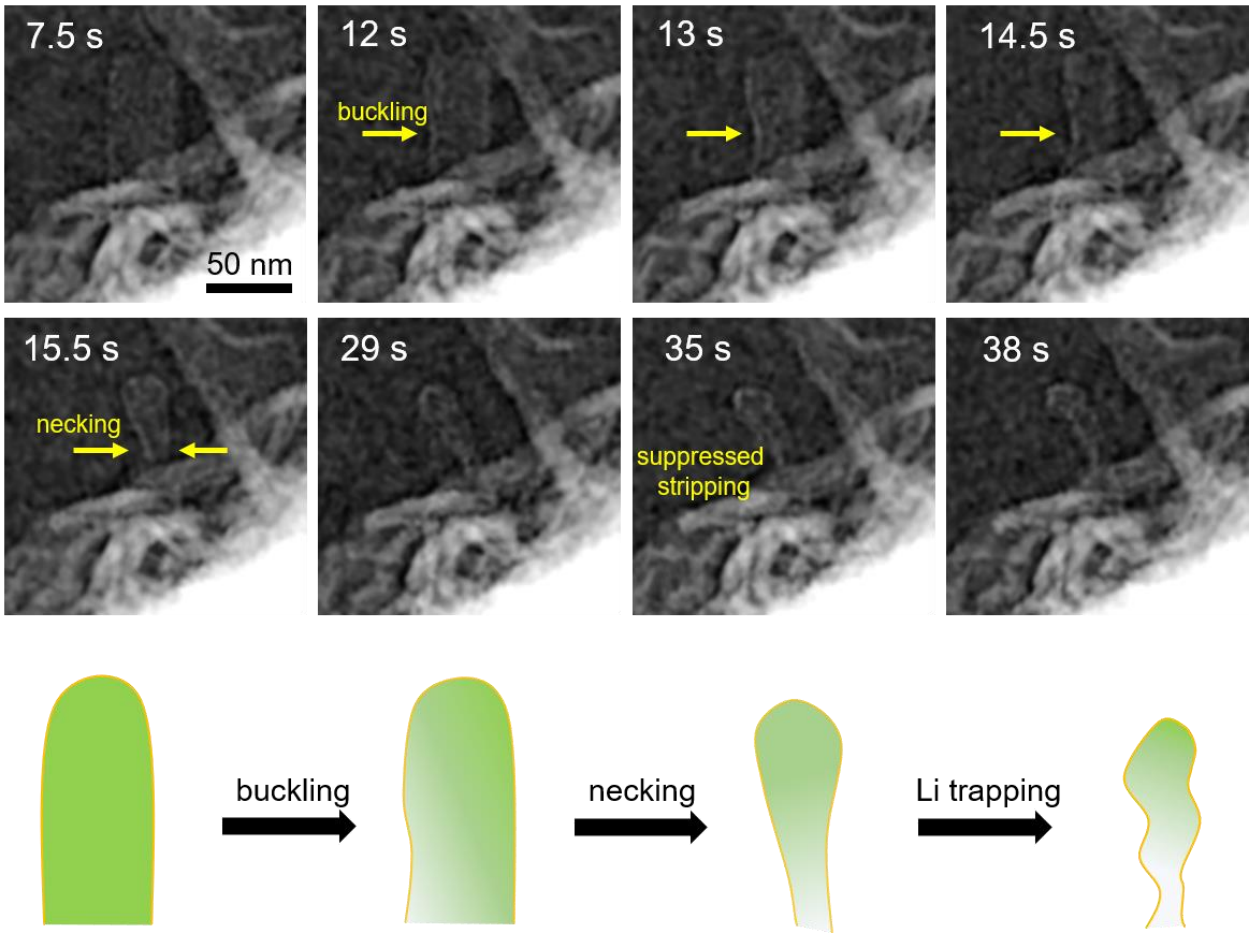

Figure S2. *In-situ* observation and schematics of Li stripping in Li_2O SEI obeying stripping Mode I. During the stripping process, Li 'trapping' was induced by severe Li_2O SEI buckling and necking. The applied bias is -5V. The t/r ratio of the whisker is 0.14.

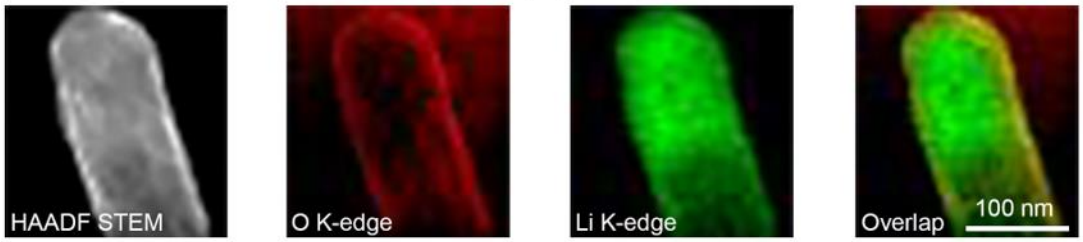

Figure S3 EELS maps of Li and O in a partly stripped Li whisker in Li_2O SEI. The O and Li maps are obtained from O-K edge and Li K-edge.

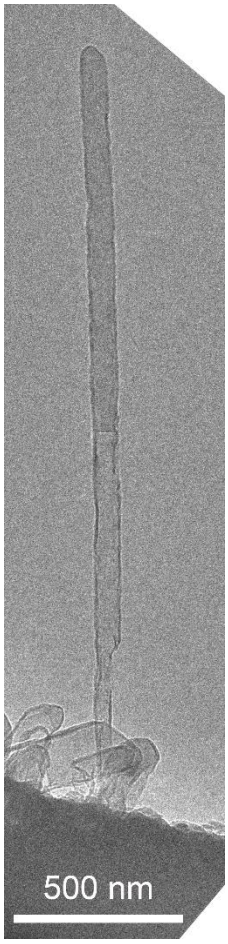

Figure S4. Mode II stripping in a long whisker with a length larger than 2µm.

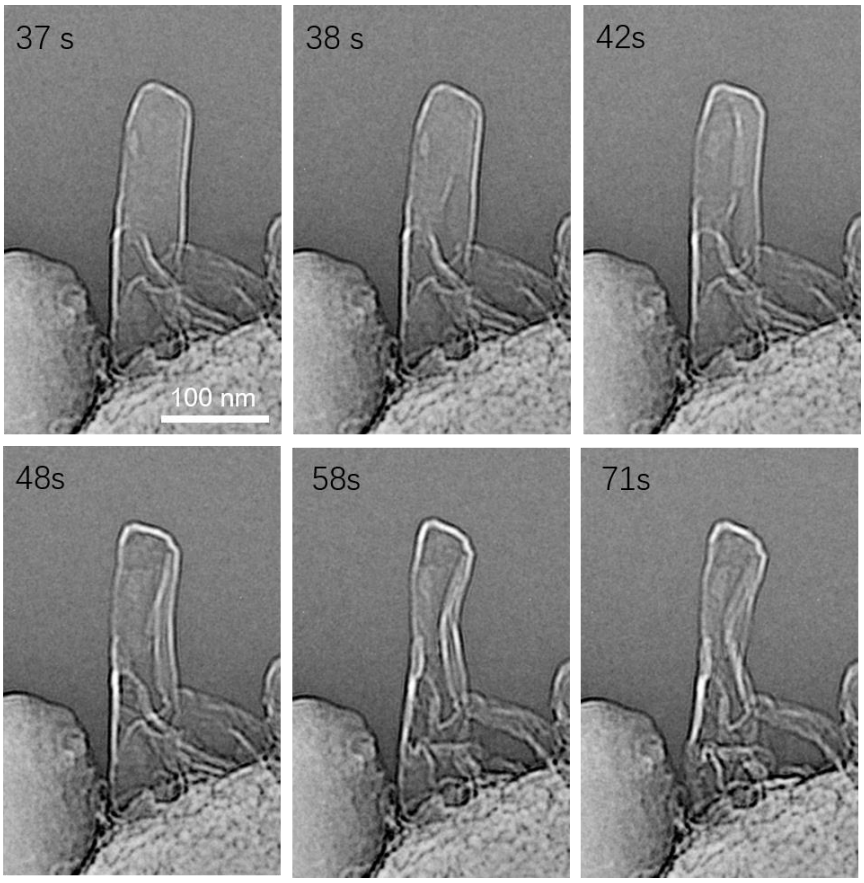

Figure S5. *In-situ* observation of Li stripping in Li_2O SEI with a critical *t/r* ratio of 0.21. During the stripping process, the Li_2O SEI underwent moderate buckling without evident necking, which is different from the stripping Mode I. Meanwhile, as the Li whisker was nearly stripped off before the buckling, no Li 'trapping' as that shown in stripping Mode II was formed.

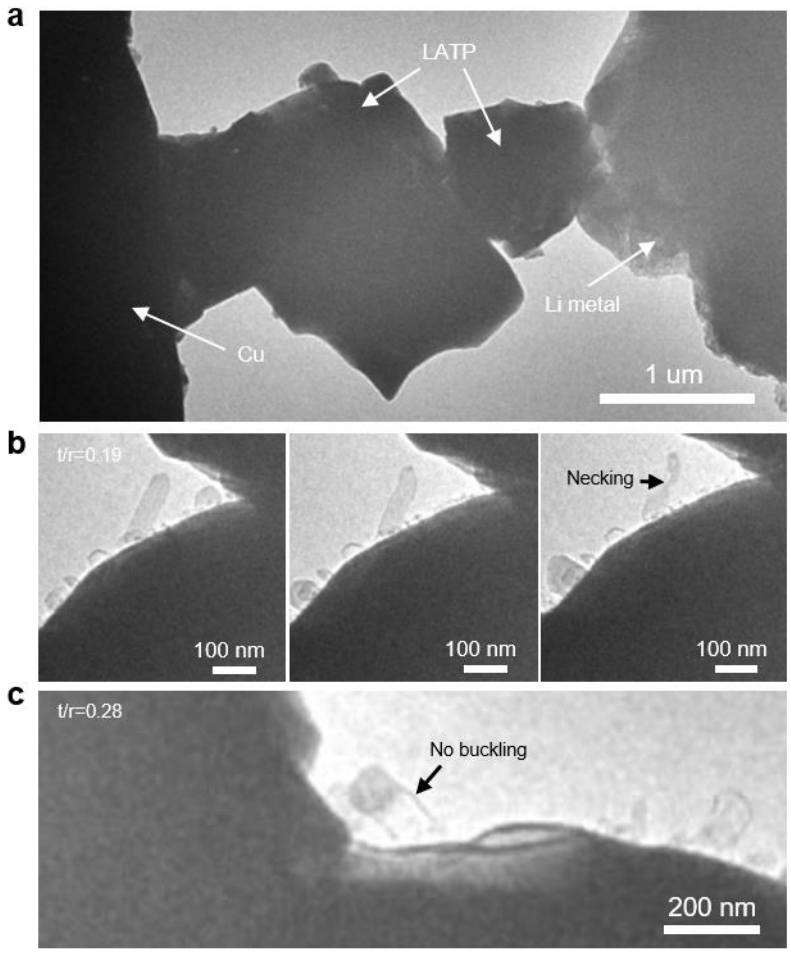

Figure S6. Direct observation of Mode I and Mode II stripping in an oxide SSE system. a, TEM set-up for the *in-situ* experiments. b,c, Mode I stripping (b) and Mode II stripping (c) observed in whiskers with different t/r ratios.

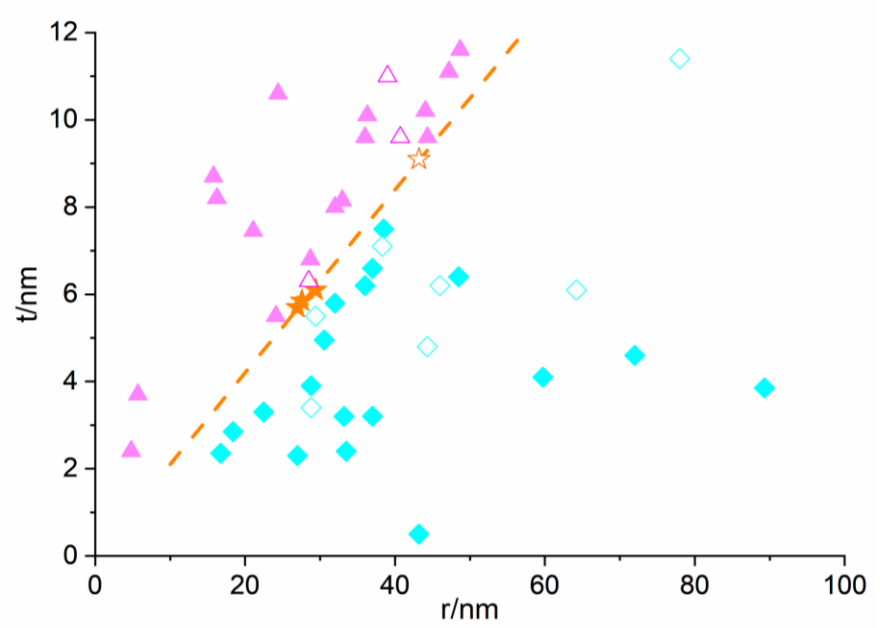

Figure S7. Statistical distribution of the two types of stripping modes. Mode Ⅰ and Mode Ⅱ are denoted by cyan diamonds and magenta triangles, respectively. Solid and hollow symbols represent data points obtained from FCNFs and oxide systems, respectively. The result shows that the mechanical criterion established in this work also applies well to the oxide SSE system.

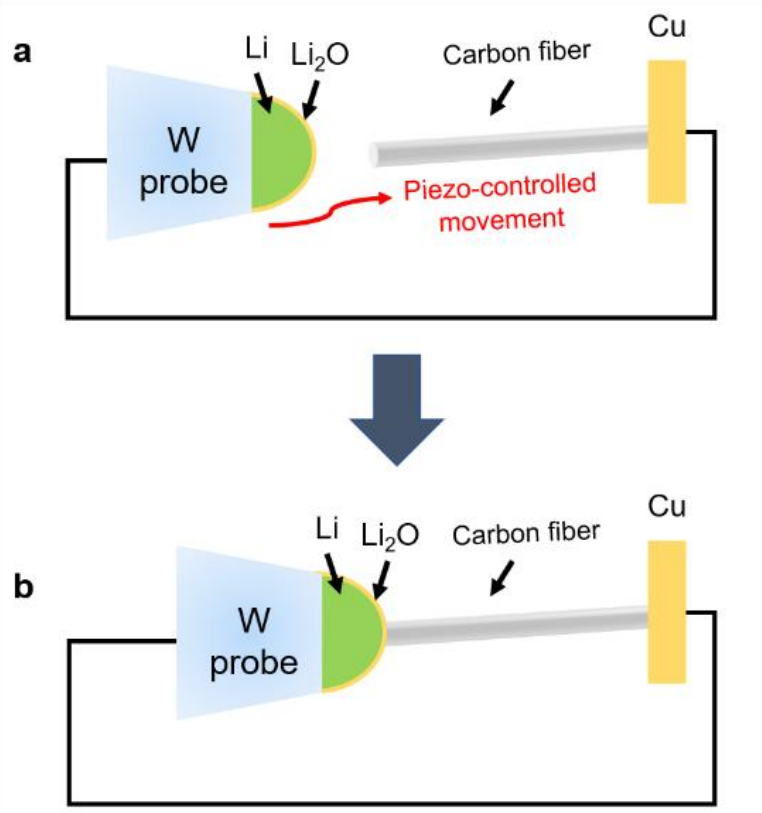

Figure S8. Schematic illustration of the experimental procedure.